A songbird compensates for wing molt during escape flights by reducing the molt gap and increasing angle-of-attack

Barbara M Tomotani[1,2,3] & Florian T Muijres[1]

[1] Experimental Zoology Group, Wageningen University & Research, PO Box 338, 6700 AH Wageningen, The Netherlands

[2] Department of Animal Ecology, Netherlands Institute of Ecology (NIOO-KNAW), PO Box 50, 6700 AB Wageningen, The Netherlands

[3] Museum of New Zealand Te Papa Tongarewa, Wellington, New Zealand

Abstract

During molt, birds replace their feathers to retain feather quality and maintain flight performance. However, wing gaps inherent of this process can also reduce flight capacities, which could be detrimental when foraging or escaping predators. Still, many bird species will not stop their normal activities when molting. In this study, we investigated whether and how birds adjust their escape flight behavior to compensate for the reduction in performance when flying with wing gaps. Using stereoscopic high-speed videography, we filmed 146 upward-directed escape flights of 19 and 22 pied flycatchers (*Ficedula hypoleuca*) with and without simulated molt gaps, respectively. We then reconstructed the three-dimensional body and wing movements throughout each maneuver. By comparing flights with and without gaps, we determined how wing molt gaps affected wing morphology, escape flight performance, and how the birds adjusted their flight kinematics in order to negate possible negative aerodynamic effects. Our manipulations resulted in a lower second-moment-of-area of the wings, but flight speed and net aerodynamic force production did not differ between the two groups. We found that in manipulated birds, the size of the gap was reduced as the flight feathers adjacent to the gap had moved towards each other. Moreover, the experimental decrease in second-moment-of-area was associated with an increase in angle-of-attack, whereas changes in wingbeat-induced speeds were associated with variations in aerodynamic force production. This suggests that the control of escape flight in molting birds might be modular, allowing relatively simple flight control, thus reducing the burden on the neuro-muscular flight control system.

Keywords: European pied flycatcher, *Ficedula hypoleuca*, avian flight, wingbeat kinematics

Introduction

The avian plumage not only functions as a protective barrier and insulation layer but is also essential for locomotion, forming the aerodynamic shape of the animal's body, tail and wings during flight. As a result, avian feathers are under strong selective pressure for optimal flight performance (Jenni and Winkler, 1994). Environmental and biological factors such as sunlight, weather and parasites cause feathers to degrade over time, reducing their quality and compromising all activities of an individual (Barbosa et al., 2002; de la Hera et al., 2010; Swaddle et al., 1996; Weber et al., 2005). Thus, birds need to replace their feathers in order to retain quality in the so-called molt process (Jenni and Winkler, 1994; Pap et al., 2007). This is particularly important for the flight feathers, as a degraded or damaged feather deck is likely to impact flight performance (Swaddle et al., 1996).

The process of molt is energetically costly because individuals need to grow new feathers and maintain tissues for feather production (Lindström et al., 1994; Murphy and King, 1991; Murphy and King, 1992). It also has to be timed correctly in the season because if molt is delayed, is hastened or when it overlaps with other stages in the annual cycle, it may compromise plumage quality (Dawson, 2004; Jenni and Winkler, 1994; Nilsson and Svensson, 1996; Vágási et al., 2012). Therefore, allocation of this expensive stage in the annual cycle of a bird is an important life-history decision (Barta et al., 2008; Hemborg et al., 2001; Holmgren and Hedenström, 1995; Jenni and Winkler, 1994).

The energetic requirements of growing new feathers, however, is not the only reason why molt is costly. During molt, birds are also forced to fly with missing wing feathers, which forms gaps on their wings and causes additional energetic costs (Chai, 1997; McFarlane et al., 2016; Swaddle and Witter, 1997; Swaddle et al., 1999; Williams and Swaddle, 2003). Such molt gaps are detrimental to bird flight due to a reduction in the wing area, altered wing shape and a consequent increase in wing loading, hindering the ability to generate aerodynamic lift or causing additional aerodynamic drag (Achache et al., 2018; Chai, 1997; Hedenström and Sunada, 1999; Kleinheerenbrink and Hedenström, 2017; McFarlane et al., 2016). Both the gap size and position are detrimental for flight, with a strong decline in performance when the gaps are situated inside the wing, which is the case of early molt stages (Achache et al., 2018; Hedenström and Sunada, 1999).

There are different strategies that individuals use to reduce the costs of molt, such as molting just one or few feathers at once and allocating molt to moments of the year when there are no other costly events such as breeding or migration (Barta et al., 2006; Barta et al., 2008; Jenni and Winkler, 1994). Still, it is not uncommon for some birds to start to molt

while still breeding even if this means that they will pay additional costs of overlapping molt and breeding (Echeverry-Galvis and Hau, 2013; Hemborg, 1999; Hemborg and Lundberg, 1998).

In a previous study, we investigated the costs of molting while breeding and showed that male pied flycatchers (*Ficedula hypoleuca*) with simulated molt gaps in their wings suffer from flight costs measured as distance gained per wingbeat, a parameter with potential energetic implications (Tomotani et al., 2018b). However, this reduction in performance did not reflect in a reduction in flight speed of birds with simulated molt gaps (Tomotani et al., 2018b). Similarly, a study with starlings showed that birds with simulated molt gaps had a low speed take-off immediately after manipulation, but that effect disappeared over time (Williams and Swaddle, 2003). These results suggest that individual birds may be able to behaviorally compensate for the detrimental effects of wing feather gaps on take-off performance (Tomotani et al., 2018b; Williams and Swaddle, 2003). Here, we investigated whether and how birds compensate for the detrimental effects of molt gaps on escape flight performance via adjustments in their flight kinematics. We studied the upward-directed escape take-off maneuvers of pied flycatchers with and without experimentally-induced gaps in their wings simulating early molt stages (henceforth "*control* group" and "*molt* group", respectively). We used video recordings of 146 escape take-off flights in a vertical flight chamber of 19 birds with simulated molt gaps and 22 *control* birds to create a dataset of the three-dimensional body and wing movements throughout the escape flight. Based on these data, we described in detail how gaps of early molt stages affect wing morphology, escape flight performance, and how pied flycatchers adjust their flight kinematics in order to negate the negative aerodynamic effects of molt.

Materials & Methods

Modelling aerodynamic force production in upward-directed escape flights

Flying animals flap their wings to produce aerodynamic forces required for flight. During steady horizontal flight, the animal needs to produce an upward-directed aerodynamic lift force that is in magnitude equal to the weight of the animal, and a forward-directed thrust force produced by the flapping wings that cancels aerodynamic drag mostly produced by the body (Alexander, 2004).

During vertical escape flights, on the other hand, the animal should maximize the upward-directed aerodynamic force (F_{aero}) in order to accelerate upwards as fast as possible.

The resulting high upward accelerations throughout an escape flight lead to a high escape speed as well as a short time duration of the escape maneuver. Both characteristics are associated with a high escape performance (Muijres et al., 2014; Swaddle et al., 1996), as they minimize the chance of being captured. Equally, these metrics could also be used to quantify capture performance in predators (Hedenstrom et al., 2001).

Because acceleration, escape speed and escape time thus all depend directly on the net aerodynamic force (F_{aero}) produced by the upward flying bird, we used this metric to quantify escape performance. To control for differences in size among the individual birds, we normalized this F_{aero} with the weight of the individual bird, leading to the weight-normalized net aerodynamic force, defined as

$$F^*_{aero} = F_{aero}/mg, \qquad\qquad\qquad \text{Eqn. 1}$$

where m is mass of the bird and g is gravitational acceleration (see Table 1 for the complete list of symbols). This net aerodynamic force (F_{aero}) equals the vector-sum of the force produced by the bird for weight support and the force that leads to body acceleration (Fig. 1B), and thus using Newton's second law of motion, we can directly determine F^*_{aero} from body accelerations as

$$F^*_{aero} = |\mathbf{a}+\mathbf{g}|/|\mathbf{g}|, \qquad\qquad\qquad \text{Eqn. 2}$$

where $\mathbf{g}$ is the gravitational acceleration vector, and $\mathbf{a}$ is the body acceleration vector. These weight-normalized aerodynamic forces are thus equal to the amount of g-forces experienced by the bird throughout the escape maneuver.

The total net aerodynamic force produced by the flying bird can be separated into forces produced by its wings, body and tail as (Fig. 1C)

$$F^*_{aero} = (F_{wings} + F_{body} + F_{tail})/mg. \qquad\qquad\qquad \text{Eqn. 3}$$

During flapping flight at low advance ratio's, such as the here-studied escape take-offs, aerodynamic forces produced by the wings (F_{wings}) result primarily from its flapping motion. Therefore, we will model aerodynamic forces produced by the wings throughout an escape take-off using aerodynamic theory for wings beating at low-advance-ratio's (Ellington, 1984; Muijres et al., 2017) as (Fig. 1C)

$$F_{\text{wings}} = \text{½} \, \rho \, \dot{\varphi}^2 \, S_2 \, \alpha_{\text{wing}} \, C_{F\alpha},$$ Eqn. 4

whereby ρ is the air density, $\dot{\varphi}$ is the angular speed of a beating wing, S_2 is the second-moment-of-area of the wing relative to the shoulder joint, α_{wing} is the angle-of-attack of the wing, and $C_{F\alpha}$ is the angle-of-attack-specific force coefficient of the wing. We model the wing force coefficient as the product of α_{wing} and $C_{F\alpha}$ because for revolving bird wings, their force coefficients scales close to linearly with angle-of-attack (Usherwood, 2009).

The forces produced by the tail (F_{tail}) can be modelled using delta-wing aerodynamics theory applied to avian tails (Thomas, 1993), as

$$F_{\text{tail}} = \frac{\pi}{4} \rho \, U_{\text{tail}}^2 \, b_{\text{tail}}^2 \, \alpha_{\text{tail}},$$ Eqn. 5

whereby U_{tail} is the tail speed resulting from both beating the tail and the translational speed of the bird, b_{tail} is the maximum tail width, and α_{tail} is the angle-of-attack of the tail.

The advance ratio of the here-studied escape take-offs are relatively low, and translation velocities of the bird are relatively small compared to wingbeat and tailbeat induced velocities. Because aerodynamic forces scale with velocities squared (Anderson, 1985), we ignore aerodynamic forces that are the result of primarily the relatively low translational velocities. Therefore, we assume that body-induced aerodynamic forces are negligible in our aerodynamic model for escape take-off maneuvers in birds ($F_{\text{body}} = 0$). Note that because wing molt most likely does not change body drag directly, even if body drag forces are not negligible, this simplification will most likely not affect our study into the effect of wing molt on flight kinematics and aerodynamics.

The aerodynamic model as described by Eqn. 1-5 will be used to study how wing molt affects the flight kinematics, aerodynamics and performance of escape take-offs in pied flycatchers. Based on this model, we hypothesize that the primary detrimental effect of wing molt is that molt gaps cause a reduction in S_2 of the wings, which will have a negative effect on force production by the wings (Eqn. 4). This could then lead to a reduction in escape flight performance as expressed by a reduction in F^*_{aero} (Eqn. 1-2). But our previous study suggests that instead of having a reduced escape performance, our molting pied flycatchers adjusted their flight kinematics in order to negate this negative effect (Tomotani et al., 2018b). Therefore, using our aerodynamic force production model for wings and tail (Eqn. 4 and Eqn.

5, respectively), we will investigate how these pied flycatchers adjusted their wingbeat and tailbeat kinematics in order to compensate for wing molt.

According to Eqn. 4, birds can increase aerodynamic forces produced of the molting wings by increasing S_2 (e.g. by spreading their remaining wing feathers), by increasing the angle-of-attack of the beating wings, and by increasing the (angular) speed of the wings. Likewise, birds can increase force production by the tail by spreading the tail (increasing b_{tail}), increasing the tail angle-of-attack, and increasing the speed of the tail (Eqn. 5). Therefore, we measured these parameters in escaping flycatchers, and tested how they vary between birds with and without simulated molt gaps. Note that, especially at relatively low flight speeds, pied flycatchers have an inactive upstroke whereby the wing does not produce significant aerodynamic forces (Muijres et al., 2012; Norberg, 1975). Therefore, we will focus on the wingbeat kinematics particularly during the aerodynamically-active downstroke.

Experimental Animals

The pied flycatcher, *Ficedula hypoleuca* ([Pallas], 1764), is a small long-distance migratory bird that reproduces in Europe and Western Asia and winters in West Africa (Lundberg and Alatalo, 1992; Ouwehand et al., 2016). The field part of the experiment was conducted from early April until late June 2015 in the forests of the Hoge Veluwe National Park (The Netherlands; 5°51'E, 52°02'N). We provided around 400 nest boxes year-round in an area of 171 ha, which are occupied in spring by cavity-nesting passerines, such as pied flycatchers. Every year this pied flycatcher population is monitored and data on arrival dates of males, nest building of females, female egg-laying dates, chick hatching dates, brood success and adults and chick basic biometrics is collected. Voucher material of this population was deposited in the ornithology collection of the Naturalis Biodiversity Center (Leiden, The Netherlands) under the inventory numbers RMNH 592347, RMNH 592348 and RMNH 592349.

Birds used in the present study were part of a previous field-lab experiment designed to test the effects of simulated molt gap on fitness (Tomotani et al., 2018b). Adult males were captured when feeding their seven-day old chicks and randomly assigned to a treatment: if a male was in the *molt* group, we simulated early molt stages by plucking primaries 2 and 3 of both wings, following the molt sequence (Jenni and Winkler, 1994). If a male was in the *control* group, it was handled as a *molt* group male, but no primary feathers were removed. Our treatment mimicked the natural molt process in pied flycatchers, with the exception that we removed primary 2 and 3, instead of 1 and 2. We opted to not remove the first primary

feather because this allowed us to assess the date of the natural molt onset as the moment when the first primary was dropped. Nevertheless, our treatment still created a similar-sized gap in a very close location to where the natural molt would start. After this experimental treatment, all birds were released. Later, when chicks were 12 days old, those males were captured a second time and taken to the Netherlands Institute of Ecology where we recorded their flight.

All procedures were carried out under licenses of the Animal Experimental Committee of the Royal Netherlands Academy of Sciences (KNAW) (protocol NIOO 14.13). The *molt* treatment consisted in pulling feathers from the wings of the males upon capture, a process that last a few seconds and was only performed by experienced researchers. Moreover, the return rates of *molt* and *control* males in the following year did not differ (see Tomotani et al, 2018b). More details regarding the design and results of this field experiment can be found in Tomotani et al. (2018b).

Experimental Setup & procedure

Escape flight experiments were performed in a vertical flight arena with a stereoscopic videography system (Fig. 1A), as described in Tomotani et al. (2018b). The flight tunnel consisted of a release chamber, a flight chamber and a collection chamber. The flight chamber had dimensions $50 \times 50 \times 150$ cm (length $\times$ width $\times$ height), and the release and collection boxes were each $50 \times 50 \times 30$ cm in size. The release and collection chambers were removable and identical in design, such that they were interchangeable and could be used as transport cage. Each cage had a perch and a sliding door (50×50 cm) that could be quickly opened manually by the experimenter.

Before each experimental session, a single bird was transferred from its housing cage to the release chamber and transported to the experimental room. There, the release chamber was connected to the bottom of the flight arena and the sliding door was quickly opened. This would trigger the bird to fly upward and land on the perch of the collection chamber on the top. After this, the experimenter would close the sliding door of the collection chamber, switched the release and collection boxes, and performed a second flight experiment by again quickly opening the sliding door of the release chamber.

The upward flight maneuvers were filmed with a stereoscopic videography system, consisting of three synchronized Basler piA64-210gm cameras, each with a Nikkor f/2.8 lens and a 300 watt halogen floodlight (GE lighting, PAR56) for illumination. Each camera had a

spatial resolution of 648 × 488 pixels, gray-scale bit depth of 8 bits, and operated at 150 or 200 frames per second (Fig. 1B, Movies S1-S2). The stereoscopic camera system was calibrated at least once a week using a Direct Linear Translation (DLT) method (Hatze, 1988), based on a calibration frame with 22 randomly placed calibration points, and using an open-source Matlab (Mathworks Inc) DLT calibration software package (Woltring and Huiskes, 1990). The accuracy of each DLT calibration was estimated as the mean absolute calibration error, defined as the mean absolute distance between the location of each calibration point and its three-dimensional reconstruction; for our study, this mean absolute calibration error was 7.5 (0.6) mm (mean (standard deviation), n=7 calibrations).

The stereoscopic camera system filmed a volume of approximately 40 × 40 × 40 cm on the bottom half of the flight chamber, and thus the mean absolute calibration error equals 1.1% of the diameter of this volume of interest. We chose to film this region in the bottom half of the flight chamber because we assumed that in this section the birds were producing maximum aerodynamic forces in order to accelerate upward. Closer to the take-off perch, the birds might still be transitioning from the push-off phase to the flight phase, and more towards the collection chamber they might start to slow down in order to prepare for landing.

During the experiments, the camera system was continuously recording to a buffer of 1000 video frames (5 or 6.7 seconds) for each camera. When the system was manually triggered after a bird performed a flight maneuver, recording was stopped and the final 1000 video frames recorded by each camera before triggering were saved and stored for later analysis (Movies S1-S2).

Flight Kinematics Analysis
Throughout each recorded stereoscopic video, we manually tracked 14 morphologically distinct markers on the body, wings and tail of the upward flying bird (Fig. 1C), using an open-source Matlab (Mathworks Inc) tracking software package (Hedrick, 2008). The body and tail markers included the tip of the beak, the rump, and the left and right tail tip. On each wing, we tracked five markers: the shoulder, the wrist, the wing tip defined as the tip of the eighth primary feather (P8), and the tip of the first and fourth primary feather (P1 and P4, respectively); P1 and P4 were adjacent to the feathers that we removed in the molt-simulated group (P2 and P3).

We used the open-source DLT calibration code (Woltring and Huiskes, 1990) to convert all video-tracked marker positions into their three-dimensional positions. For each of

these three-dimensional reconstructions, we determined the mean absolute reconstruction error, defined as the mean distance between the measured location of a marker on each camera sensor and the re-projected location on the camera sensor of the estimated three-dimensional marker position. For all three-dimensional reconstructions, the mean absolute reconstruction error is 2.7 (2.6) pixels (mean (standard deviation), n=39,503 reconstructions), which equals 0.3% of the diameter of each camera sensor.

The resulting three-dimensional tracks were filtered using a linear Kalman smoother (Muijres et al., 2015), which provided us with filtered estimates of position, velocity and acceleration of all data points. For the Kalman smoother, the measurement noise covariance matrix was set to identity, process noise matrix set to 10, and the cross-product of the error covariance matrices was set to zero. A comparison between the unfiltered and Kalman filtered data of a flight maneuver is shown in Fig. S1.

These filtered data were used to determine the various kinematics parameters throughout each measured wingbeat. We first separated each flight sequence into distinct wingbeats, by manually identifying the video frames at which the wingbeat transitioned from downstroke to upstroke, i.e. when the wingtip switched from a downward to upward movement. Based on this, we defined the temporal dynamics throughout the wingbeat as normalized time $\tau = t/\Delta t$, whereby Δt was the time difference between two consecutive downstroke-to-upstroke transitions. And thus τ=0 at the start of each upstroke, and τ =1 at the end of the next downstroke. The flapping frequency of each wingbeat was calculated as $f = 1/\Delta t$. We used the tip of the beak to determine the flight path, flight speed $U_{\text{body}}(\tau)$ and weight-normalized net aerodynamic force $F^*_{\text{aero}}(\tau)$ (Eqn. 2), throughout each wingbeat.

More detailed wingbeat kinematics analysis was performed by dividing the wing into four triangles, each spanned by three tracked markers (Fig. 1C): the inner wing triangle T_{in}, the mid wing triangle T_{mid}, the outer wing triangle T_{out}, and the simulated molt gap triangle T_{gap}. Thus, for the *molt* group, the molt gap was defined as the triangle spanned by the shoulder joint and the wing tips of feathers P1 and P4, and simulated molt gap width (b_{gap}) as the distance between the tip of P1 and P4.

For each wing triangle we calculated its area S, second-moment-of-area S_2 relative to the shoulder marker, its velocity vector **U** as the average velocity of its three markers, and angle-of-attack α as the angle between the velocity vector **U** and the surface of the triangle (Fig. 1C). The average wing speed U_{wing} and angle-of-attack α_{wing} for the bird were estimated as the average speed and angle-of-attack of the inner, middle and outer wing triangles of both

wings combined. For *control* birds without a simulated molt gap, total wing area and S_2 were estimated as the sum of S and S_2 for all the wing triangles of both wings combined, respectively. For birds with simulated molt gaps, the gap triangles were not included in the S and S_2 calculation.

We defined the tail as a triangle spanned by the rump marker and the two tail tips. From this tail triangle, we calculated tail velocity $\mathbf{U}_{tail}$ and tail angle of attack α_{tail}, using the same method as for the wing triangles (Fig. 1C). Tail width b_{tail} throughout each wingbeat was calculated as the distance between the two tail tip markers.

Statistical Analysis

All statistics were performed using R version 3.4.3 (R Core Team, 2017). We tested how wing molt affected upward-directed flight dynamics of pied flycatchers using linear mixed-effect models. Mixed-effect models were fitted to each flight performance, morphology and kinematics component (R packages "lme4", Bates et al., 2015) as a response variable, with "treatment" as fixed effect and bird ID as a random effect to take into account that each individual was tested multiple times. Treatment effects were tested using a Kenward-Roger approximation for F-tests, comparing models with and without treatment (R function "KRmodcomp" from the "pbkrtest" package, Halekoh and Højsgaard, 2014); data did not violate model assumptions and critical *p*-values were subsequently corrected for multiple testing using a Holm-Bonferroni method (Holm, 1979).

The tested flight performance, morphology and kinematics components included all variables identified as important for aerodynamic force production in upward-directed avian flight (Fig. 1C). The flight performance metrics were flight speed and weight-normalized net aerodynamic force; the wing morphology parameters were molt gap size and second-moment-of-area of both wings combined; the wingbeat kinematics parameters were the average wing speed and angle-of-attack of both wings combined (Eqn. 4); the tail kinematics parameters tail speed, tail angle-of-attack and tail spread (Eqn. 5).

For the flight performance metrics flight speed and normalized force, we used the wingbeat average values. For all other parameters, we used the average values near the moment within the wingbeat when force production was maximum ($F^*_{aero} \approx F^*_{aero,max}$). This was around mid-downstroke, within the wingbeat-normalized time window of $0.5 < \tau < 0.6$. Our rational for analyzing the kinematics parameters near maximum force production is that

in this time window the effect of these parameters on flight performance are also most likely maximum (Eqn. 4,5).

To test which flight kinematic components best explain the force production, we used a linear mixed-effect model with normalized force as response variable and with second-moment-of-area, flight speed, wing speed, wing angle-of-attack, tail speed, tail spread and tail angle-of-attack as fixed effects, again using bird ID as a random effect. To define the minimal model, we used backwards model selection, dropping non-significant terms in each step. Once more, effects were compared with a Kenward-Roger approximation for F-tests.

In addition to the isolated comparisons, we also carried out a principal component analysis (PCA) to visualize all metrics together. The PCA reduces the number of dimensions of data by geometrically projecting the data into lower dimensions (principal components, PCs). It thus reduces the complexity of high-dimensional data but retain trends and patterns (Jolliffe, 2002; Lever et al., 2017). All analyzed metrics were included in order to detect whether data of the two treatments would cluster and which metric(s) would be related to the treatment effects. The Principal Component Analysis was based on the standardized measurement values (mean centered at 0, standard deviation at 1) of the variables.

Results

Pairs of *control* and *molt* males (*n*=29 pairs, 58 males) with the same hatch date and same brood sizes were selected throughout the season covering the full range of hatching dates. This ensured that the treatment groups did not significantly differ on average chick hatching date or in brood size (see Tomotani et al, 2018b). From these starting 58 nests, however, we analyzed recordings of 41 males; the remaining birds were either not recorded (*e.g.* natural molt, desertion, see Tomotani et al, 2018b) or recordings were not precise enough for tracing the whole wing movement. However, this subset of nests still did not differ in terms of brood sizes ($F_{1,40}$=-1.30, *p*=0.20) nor in hatching dates ($F_{1,40}$=2.48, *p*=0.80).

Based on 10 years of molt data, male pied flycatchers in this population start to symmetrically molt on the June 13th on average (Tomotani et al, 2018a). In the year of the experiment (2015), males started to molt on average on June 15th, while flight trials took place between May 28th and June 18th. Natural molt onset was monitored in all individuals and was not affected by treatment; individuals observed in natural molt prior to flight trials were excluded from all analyses (also see Tomotani et al, 2018b).

We recorded and analyzed 73 upward-directed escape flight sequences of 22 *control* birds, and 73 sequences of 19 birds with simulated molt gaps (see Movies S1 and S2 for respective example videos). By manually tracking the 14 body, wing and tail markers in 4147 frames of these 146 stereoscopic videos, we determined the wing, body and tail kinematics throughout a total of 410 complete wingbeats (Database S1).

Changes in flight performance as a result of molt

The flight speed of the *control* birds and birds with simulated molt gaps varied throughout the wingbeat, with a consistent offset in flight speed between the *control* and *molt* group (Fig. 2A). Despite this offset, the average flight speed throughout the wingbeat was not significantly different between the two groups ($U_{body,control}$=2.53±0.03 m s^{-1} (mean±standard error, *n*=73 flights); $U_{body,molt}$=2.47±0.03 m s^{-1} (*n*=73 flights); F$_{1,38.48}$=0.94, *p*=0.34; Fig. 2E), and thus both the *control* and *molt* group flew upward with a flight speed of approximately 2.5 m s^{-1}.

The net weight-normalized aerodynamic forces also varied throughout the wingbeat, and these dynamics were strikingly similar between the *control* and the *molt* groups (Fig. 2B): for all birds, normalized forces increased on average from a g-force of 1.6 at the start of the wingbeat (τ=0) to a maximum of 2.6 g near mid downstroke (τ≈0.55). The resulting wingbeat-average normalized forces were not significantly different between the two groups ($F^*_{aero,control}$=2.16±0.05 (*n*=73 flights); $F^*_{aero,molt}$=2.09±0.05 (*n*=73 flights); F$_{1,37.89}$=0.69, *p*=0.41; Fig. 2F). Thus, throughout the escape maneuver, both the *control* and *molt* birds produced similar net aerodynamic forces of on average 2.1 g, and that peaked near mid-downstroke at a value of 2.6 g.

Changes in wing morphology as a result of molt

Based on the tracked wing markers, we measured the temporal dynamics of second-moment-of-area of both wings combined throughout the wingbeat (Fig. 2C). Because the wing markers are only clearly visible during its downstroke movement, we were only able to accurately estimate S_2 (and any other wing kinematics parameter) within the time window of 0.25<τ<0.8. Within this time window, the second-moment-of-area first slowly increased to a maximum at roughly mid-downstroke (τ~0.5), and then dropped off towards the end of the downstroke. Throughout the complete measured wingbeat section, the second-moment-of-area was larger for the *control* group than for the *molt* group (Fig. 2C); also, the average

second-moment-of-area near maximum force production ($0.5<\tau<0.6$) was significantly higher for the *control* birds ($S_{2,control}$=1.61±0.05 dm^4 (n=66 flights); $S_{2,molt}$=1.28±0.04 dm^4 (n=65 flights), $F_{1,35.72}$=20.61, $p<0.01$; Fig. 2G). These results show that the birds with simulated molt had wings with a 20% lower second-moment-of-area compared to the *control* group.

We tested how this reduction in second-moment-of-area relates to the introduction of the molt gap by comparing the distance between the tips of primary feathers P1 and P4, which for the birds in the *molt* group is representative of the simulated molt gap width (Fig. 1C). This P1-P4 distance was on average 31% larger for the *control* birds than for the birds with simulated molt gaps ($b_{gap,control}$=5.20±0.08 cm (n=66 flights) and $b_{gap,molt}$=3.55±0.14 cm (n=65 flights), $F_{1,37.41}$=48.59, $p<0.01$, Fig. 2D,H), and thus the birds with molt gaps had a reduced size of this gap. This molt gap reduction partly negated the detrimental effect of molt on the second-moment-of-area of the wing.

Changes in flight kinematics as a result of molt
The molt-induced reduction in second-moment-of-area causes that the birds in the *molt* group have less S_2 available to produce the same aerodynamic forces (Eqn. 4, Fig. 2). To achieve this, birds with a simulated molt gap should adjust their wing and tail kinematics. We tested how the birds in the *molt* group do this by comparing wing and tail kinematics between the two groups.

Birds can increase aerodynamic forces produced by their tail, by adjusting the spread, speed and angle-of-attack of the tail (Eqn. 5), and thus we tested those three parameters. None of these differed significantly between the *molt* and *control* groups (Table S1), suggesting that pied flycatchers do not use their tail to compensate for wing molt ($U_{tail,control}$=3.63±0.07 m s^{-1} (n=72 flights), $U_{tail,molt}$=3.41±0.05 m s^{-1} (n=73 flights), $F_{1,38.46}$=1.89, p=0.18; $b_{tail,control}$=5.25±0.23 cm (n=72 flights), $b_{tail,molt}$=5.08±0.26 cm (n=73 flights), $F_{1,37.77}$=0.15, p=0.70; $\alpha_{tail,control}$=32.1º±1.76º (n=72 flights), $\alpha_{tail,molt}$=33.94º±2.07º (n=73 flights), $F_{1,38.47}$=0.47, p=0.50).

Birds can increase the aerodynamic forces produced by their flapping wings primarily by increasing the wing speed and by adjusting the angle-of-attack (Eqn. 4). The temporal dynamics of wing speed throughout the wingbeat is similar between the birds in the *control* and *molt* groups: the speed of the inner wing section remains roughly constant throughout the downstroke (Fig. 3A); the speed of the middle wing section slowly increases throughout the downstroke (Fig. 3B); for the outer wing triangle, the wing speed first increases to a

maximum of roughly 12 m s^{-1} at τ=0.4, after which it decreases again (Fig. 3C). Although their temporal dynamics is similar between the *control* and *molt* group, the speeds are on average higher for the birds with simulated molt gaps (Fig. 3), which is also the case for the average speed of the complete wing (Fig. 4A). Comparing the average wing speed at maximum force production between the *control* and *molt* groups shows that the average speed was not significantly different between the groups ($U_{\text{wing,control}}$=6.52±0.16 m s^{-1} (n=66 flights) and $U_{\text{wing,molt}}$=7.00±0.16 m s^{-1} (n=65 flights), $F_{1,35.08}$=4.28, p=0.05; Fig. 4C).

The temporal dynamics of the angle-of-attack throughout the wingbeat also differed between the *control* and *molt* groups (Fig. 3D-F), particularly near mid downstroke when force production is maximal (0.5<τ<0.6). Around this phase, the angle-of-attack dips for all wing sections of both groups, but this dip is consistently less pronounced in the *molt* group (Fig. 3D-F). The same difference is observed for mean angle-of-attack of the complete wing (Fig. 4B), and as a result the average wing angle-of-attack at maximum force production is significantly higher for birds with a simulated molt gap ($\alpha_{\text{wing,control}}$=19.4°±0.8° ($n$=66 flights) and $\alpha_{\text{wing,molt}}$=23.7°±0.8° ($n$=65 flights), $F_{1,33.20}$=15.78, p<0.01; Fig. 4D).

Changes in flight kinematics for varying aerodynamic force production
Independent of molt treatment, the different birds produced various amounts of mean normalized forces throughout their maneuvers (Fig. 5). This allowed us to test how these birds adjusted their wingbeat kinematics for controlling their aerodynamic force production during upward-directed escape maneuvers. When testing for the variables that explain the variation in normalized force production, only flight speed, wing speed and tail spread relate significantly to force (Fig. 5A-C, Table S2: normalized force per flight speed slope=0.53±0.14 m^{-1} s, $F_{1,99.62}$=13.98, p<0.01; normalized force per wing speed slope=0.08±0.03 m^{-1} s, $F_{1,126.86}$=6.12, p=0.01; normalized force per tail spread slope=0.07±0.02 cm^{-1}, $F_{1,120.81}$=16.70, p<0.01). Thus, birds that flew faster also produced higher normalized forces, suggesting that these birds work harder throughout the escape maneuver. The results also suggest that normalized forces are enhanced by increasing the wing flapping speed (a g-force increase of 0.08 per 1 m s^{-1} wing speed increase) and by increasing tail spread (a g-force increase of 0.07 per 1 cm increase in tail spread). Striking is that normalized force is not related to wing angle-of-attack (slope<0.01±0.01 cm^{-1}, $F_{1,121.94}$=0.44, p=0.51).

Principal component analysis

We retained the principal components (PCs) with variance above l, leaving us with the first three PCs that, combined, explained 58% of the variation. All these three PCs differed significantly between *control* and *molt* (PC1: $F_{1,38.45}=6.88$, $p=0.01$; PC2: $F_{1,38.00}=5.80$, $p=0.02$; PC3: $F_{1,37.83}=26.32$, $p<0.01$; Tables S3, S4), but only PC2 and PC3 explained the variation of S_2 (Table S2).

When the first three principal components are represented in the biplots PC1-PC2 and PC1-PC3 (Fig. 6), there is a clear clustering of birds in *control* and *molt* groups, albeit with some overlap. This clustering is mostly evident along PC2 and PC3 axes (Fig. 6A,B). The vector (loadings) plots are consistent on showing that birds in the *molt* group are characterized by lower values of S_2, lower values of gap size and higher values of wing angle-of-attack (Fig. 6C,D). The wing angle-of-attack vector is oriented in the opposite direction of the second-moment-of-area and gap size vectors, which supports the results of the separate tests: birds with a smaller S_2 operate at higher wing angle-of-attack.

In contrast, PC1 mostly explains the variation of the normalized force, flight speed and wing speed, with all vectors pointing in a similar direction (Fig. 6C,D). In these plots, the normalized force and wing speed vectors were both close to perpendicular to the *control* and *molt* group distributions. This is in support of the above analysis that the upward escaping birds increase wing speed to enhances normalized force production, and not to control for molt.

Discussion

The study of aerodynamic effects of molt has received relatively little attention, with few studies looking at the effects of natural molt on take-off (McFarlane et al., 2016; Swaddle and Witter, 1997; Williams and Swaddle, 2003), gliding (Kleinheerenbrink and Hedenström, 2017; Tucker, 1991) or hovering flight (Achache et al., 2018; Chai, 1997). Here, we tested how experimentally-induced wing molt affects the upward-directed escape flight performance of a passerine bird after a week of habituation, and how these birds have adjusted their flight kinematics in response to molt.

Our results show that, after habituation, birds with simulated molt gaps are able to maintain their escape flight speed and aerodynamic force production via behavioral adjustments of their flight dynamics. These behavioral adjustments consist of two aspects: an adjustment of wing morphology and a change in wingbeat kinematics.

Wing molt gaps lead to a reduction in the second-moment-of-area of the wing, which consequently reduces aerodynamic force production during flight at low advance ratios (McFarlane et al., 2016). For our experimental birds, this molt-induced decrease in S_2 was partly compensated for by a reduction in the size of the molt gap. This was similarly demonstrated for gliding flight in a jackdaw (*Corvus monedula*), which modified its wing posture across molt stages in order to reduce the molt gap size (Kleinheerenbrink and Hedenström, 2017). Because there was still a molt gap present between P1 and P4, the reduction in molt gap size is not likely to be the result of feather interlocking after preening. One possibility is that the gap reduction is achieved actively via muscle tension, another possibility is a passive closure due to the lack of support from boundary feathers once they are dropped. In any case, the result is an adjustment in wing morphology, which allow molting birds to partly negate the detrimental reduction in second-moment-of-area caused by molt.

Because wing morphing only partly negated this molt-induced reduction in S_2, the molting birds needed to also adjust their flight kinematics to fully compensate for the reduction in flight performance. This could be achieved by adjusting both the wingbeat and the tail kinematics. None of the tested tail kinematics parameters significantly differed between the *molt* and *control* groups, suggesting that the tail did not contribute to this kinematics compensation. These results are in line with several previous studies showing a relative small effect of tail dynamics on aerodynamic force production in passerines (Johansson and Hedenström, 2009; Muijres et al., 2012), but they contradict models that show an important contribution of the tail to lift (Norberg, 1994; Thomas, 1993; Thomas, 1996).

Throughout the wingbeat, the wings of molting birds operated at both higher wing speeds and higher angles-of-attack (Fig. 4A,B, respectively), but the average wing speed at mid downstroke was not significantly different between the *control* and *molt* groups (Fig. 4C). In contrast, the average wing angle-of-attack at mid downstroke was significantly different between these groups (Fig. 4D). This suggests that molting birds primarily increase the angle-of-attack of the wing near mid-downstroke to compensate for the molt-induced reduction in second-moment-of-area.

Among the different analyzed flights, we observed variations not only in the second-moment-of-area, but also in aerodynamic forces magnitudes (Fig. 5). The latter variation on our data allowed us to determine how our upward escaping birds adjust their flight kinematics to control their aerodynamic force production. The analysis showed that

aerodynamic force production was positively correlated with wing speed and tail spread, suggesting that birds use these two metrics to control aerodynamic force production.

The above conclusions are supported by our principal component analysis that showed that wing speed and normalized force were both primarily associated with the first principal component, whereas S_2 and wing angle-of-attack were both primarily associated with the second and third principal components (Fig. 6, Jolliffe, 2002). The principal component analysis therefore gives some insights into the flight control mechanisms during upward escape maneuvers. These results point to a relatively simple and modular flight control system, whereby the kinematics adjustments for varying aerodynamic forces and for molt gap control are mostly independent: to compensate for a reduction in S_2, an upward escaping bird primarily adjusted the wing angle-of-attack at mid downstroke, whereas to boost aerodynamic force production the bird increases the wingbeat-induced velocities. This modularity might possibly reduce the burden on the neuro-muscular flight control system (Dickinson and Muijres, 2016; Lentink et al., 2007; Tobalske and Dial, 1994), but testing this would require additional research.

Molt is a complex process that involves tissue regeneration that impact both the energy balance and behavior. Therefore, it is also important to look experimentally at the effects of flying with molt gaps separately from the physiological costs of molt (Swaddle and Witter, 1997; Swaddle et al., 1999). A few experiments looked at the effect of simulated molt on flight dynamics of starlings (*Sturnus vulgaris*) and sparrows (*Passer montanus*). They showed that birds with simulated molt gaps have a slower take-off speed and impaired predator evasion and maneuverability as well as changes in their body mass and behavior (Lind, 2001; Lind et al., 2004; Swaddle and Witter, 1997; Swaddle et al., 1996; Swaddle et al., 1999). Curiously, after this initial impact, Swaddle and Witter (1997) also report a slow recovery of flight performance, which hints a compensatory behavior, like changes in the pattern of the wing movement. Our results support this observation. The pied flycatchers used in the present study were tested one week after being manipulated in order to also measure the impacts of our manipulations on fitness (Tomotani et al., 2018b). This may have given the birds the opportunity to adjust their behavior to retrieve the same flight speed as the controls, and for us to assess the compensation mechanism.

The study of flight performance of molting birds may help us to understand the variation of molt strategies, for example the segregation of molt from other annual cycle stages (Bridge, 2011; Tomotani et al., 2018a; Tomotani et al., 2018b). Molt may force birds to avoid costly and risky activities as the combined aerodynamics and physiological costs of

molt could be too damaging to allow molt to co-occur with other stages (Swaddle and Witter, 1997). Still, molt-breeding overlap is common in male but not female songbirds (Jenni and Winkler, 1994).

Our results suggest that, after a habituation period of one-week, early stages of molt do not negatively affect escape speed and aerodynamic force production. This is achieved by the molting birds by primarily increasing the wing angle-of-attack with approximately 4° at mid downstroke. Nevertheless, the wing molt gaps and associated wingbeat kinematics adjustments are expected to incur energetic costs: a molt gap locally reduces lift produced by that wing section, causing a dip in the spanwise lift force distribution. This decreases span efficiency and consequently increases induced drag (Hedenström and Sunada, 1999; Muijres et al., 2011); because an increase in angle-of-attack is associated with increased aerodynamic drag on the wing, the energetic power requirement for flight is expected to also increase as a result of molt-induced wingbeat kinematics adjustments (Usherwood, 2009). Thus, the detrimental effect of molt on flight performance in passerines may not be expressed in a reduction in escape speed, but instead in an increase in energetic cost of flight.

Flycatchers forage on the wing by catching insects using rapid flight maneuvers similar to the upward-directed maneuvers that we studied (Davies, 1977). Our results suggest that primarily the energetic costs such maneuvers are increased, and less so their swiftness. The resulting increase in the energetic costs of foraging and predator escape would force the males with molt-breeding overlap to allocate more energy to self-maintenance, and consequently less to their offspring. This notion helps to explain the observed response of our male pied flycatchers with molt-breeding overlap (Tomotani et al., 2018b): the *molt* group did not have a reduced fitness in terms of breeding success and next-year return rate compared to the *control* males, but males with simulated molt gaps did reduce parental care by visiting their nest fewer times, which their females compensated for by working harder. Thus, the increased power requirement of flight with molt gaps, forced males with molt-breeding overlap to prioritize their own survival (future reproduction) over their current reproduction success, which may come at the expense of their female partner (Hemborg, 1998; Hemborg, 1999; Hemborg and Merila, 1998; Tomotani et al., 2018b).

Data availability

Database S1 is available from the Dryad Digital Repository with doi:10.5061/dryad.g28t010.

References

Achache, Y., Sapir, N. and Elimelech, Y. (2018). Hovering hummingbird wing aerodynamics during the annual cycle. II. Implications of wing feather moult. *Open Sci.* **5**, 171766.

Alexander, D. E. (2004). *Nature's flyers: birds, insects, and the biomechanics of flight*. Baltimore, Maryland: Johns Hopkins Univ Pr.

Anderson, J. D. (1985). *Fundamentals of Aerodynamics*. McGraw-Hill New York.

Barbosa, A., Merino, S., Lope, F., Møller, A. P. and Moore, F. (2002). Effects of feather lice on flight behavior of male barn swallows (hirundo rustica). *The Auk* **119**, 213–216.

Barta, Z., Houston, A. I., McNamara, J. M., Welham, R. K., Hedenström, A., Weber, T. P. and Feró, O. (2006). Annual routines of non-migratory birds: Optimal moult strategies. *Oikos* **112**, 580–593.

Barta, Z., McNamara, J. M., Houston, A. I., Weber, T. P., Hedenström, A. and Feró, O. (2008). Optimal moult strategies in migratory birds. *Philos. Trans. R. Soc. Lond. B. Biol. Sci.* **363**, 211–229.

Bates, D., Mächler, M., Bolker, B. and Walker, S. (2015). Fitting Linear Mixed-Effects Models Using lme4. *J. Stat. Softw.* **67**, 1–48.

Bridge, E. S. (2011). Mind the Gaps: What's Missing in our Understanding of Feather Molt. *The Condor* **113**, 1–4.

Chai, P. (1997). Hummingbird hovering energetics during moult of primary flight feathers. *J. Exp. Biol.* **200**, 1527–1536.

Davies, N. (1977). Prey selection and the search strategy of the spotted flycatcher (Muscicapa striata): a field study on optimal foraging. *Anim. Behav.* **25**, 1016–1033.

Dawson, A. (2004). The effects of delaying the start of moult on the duration of moult, primary feather growth rates and feather mass in Common Starlings *Sturnus vulgaris*. *Ibis* **146**, 493–500.

de la Hera, I., Hedenström, A., Pérez-Tris, J. and Tellería, J. L. (2010). Variation in the mechanical properties of flight feathers of the blackcap Sylvia atricapilla in relation to migration. *J. Avian Biol.* **41**, 342–347.

Dickinson, M. H. and Muijres, F. T. (2016). The aerodynamics and control of free flight maneuvers in Drosophila. *Philos. Trans. R. Soc. Lond. B* **371**, 20150388.

Echeverry-Galvis, M. A. and Hau, M. (2013). Flight Performance and Feather Quality: Paying the Price of Overlapping Moult and Breeding in a Tropical Highland Bird. *PLoS ONE* **8**,.

Ellington, C. P. (1984). The aerodynamics of hovering insect flight. III. Kinematics. *Philos. Trans. B* **305**, 41.

Halekoh, U. and Højsgaard, S. (2014). A Kenward-Roger Approximation and Parametric Bootstrap Methods for Tests in Linear Mixed Models - The R Package pbkrtest. *J. Stat. Softw.* **59**, 1–30.

Hatze, H. (1988). High-precision three-dimensional photogrammetric calibration and object space reconstruction using a modified DLT-approach. *J. Biomech.* **21**, 533–538.

Hedenström, A. and Sunada, S. (1999). On the aerodynamics of moult gaps in birds. *J. Exp. Biol.* **202**, 67–76.

Hedenstrom, A., Rosen, M., Hedenström, A., Rosen, M. and Rosén, M. (2001). Predator versus prey: on aerial hunting and escape strategies in birds. *Behav. Ecol.* **12**, 150.

Hedrick, T. L. (2008). Software techniques for two- and three-dimensional kinematic measurements of biological and biomimetic systems. *Bioinspir. Biomim.* **3**, 034001.

Hemborg, C. (1998). Sexual differences in the control of postnuptial moult in the pied flycatcher. *Anim. Behav.* **56**, 1221–1227.

Hemborg, C. (1999). Sexual differences in moult–breeding overlap and female reproductive costs in pied flycatchers, *Ficedula hypoleuca*. *J. Anim. Ecol.* **68**, 429–436.

Hemborg, C. and Lundberg, A. (1998). Costs of overlapping reproduction and moult in passerine birds: An experiment with the pied flycatcher. *Behav. Ecol. Sociobiol.* **43**, 19–23.

Hemborg, C. and Merila, J. (1998). A Sexual Conflict in Collared Flycatchers, *Ficedula albicollis*: Early Male Moult Reduces Female Fitness. *Proc. Biol. Sci.* **265**, 2003–2007.

Hemborg, C., Sanz, J. J. and Lundberg, A. (2001). Effects of Latitude on the Trade-off between Reproduction and Moult: A Long-Term Study with Pied Flycatcher. *Oecologia* **129**, 206–212.

Holm, S. (1979). A Simple Sequentially Rejective Multiple Test Procedure. *Scand. J. Stat.* **6**, 65–70.

Holmgren, N. and Hedenström, A. (1995). The scheduling of molt in migratory birds. *Evol. Ecol.* **9**, 354–368.

Jenni, L. and Winkler, R. (1994). *Moult and ageing of European passerines*. London: Academic Press.

Johansson, L. C. and Hedenström, A. (2009). The vortex wake of blackcaps (*Sylvia atricapilla* L.) measured using high-speed digital particle image velocimetry (DPIV). *J. Exp. Biol.* **212**, 3365–76.

Jolliffe, I. T. (2002). *Principal Component Analysis*. 2nd ed. New York: Springer-Verlag.

Kleinheerenbrink, M. and Hedenström, A. (2017). Wake analysis of drag components in gliding flight of a jackdaw (*Corvus monedula*) during moult. *Interface Focus* **7**, 20160081.

Lentink, D., Müller, U. K., Stamhuis, E. J., de Kat, R., van Gestel, W., Veldhuis, L. L. M. L. M., Henningsson, P., Hedenström, A., Videler, J. J. and Van Leeuwen, J. L. (2007). How swifts control their glide performance with morphing wings. *Nature* **446**, 1082–5.

Lever, J., Krzywinski, M. and Altman, N. (2017). Points of Significance: Principal component analysis. *Nat. Methods* **14**, 641–642.

Lind, J. (2001). Escape flight in moulting Tree Sparrows (*Passer montanus*). *Funct. Ecol.* **15**, 29–35.

Lind, J., Gustin, M. and Sorace, A. (2004). Compensatory bodily changes during moult in Tree Sparrows *Passer montanus* in Italy. *Ornis Fenn.* **81**, 75–83.

Lindström, Å., Daan, S. and Visser, G. H. (1994). The conflict between moult and migratory fat deposition: A photoperiodic experiment with bluethroats. *Anim. Behav.* **48**, 1173–1181.

Lundberg, A. and Alatalo, R. V. (1992). *The Pied Flycatcher*. London: T. & A. D. Poyser.

McFarlane, L., Altringham, J. D. and Askew, G. N. (2016). Intra-specific variation in wing morphology and its impact on take-off performance in blue tits (*Cyanistes caeruleus*) during escape flights. *J. Exp. Biol.* **219**, 1369–1377.

Muijres, F. T., Spedding, G. R., Winter, Y. and Hedenström, A. (2011). Actuator disk model and span efficiency of flapping flight in bats based on time-resolved PIV measurements. *Exp. Fluids* **51**, 511–525.

Muijres, F. T., Bowlin, M. S., Johansson, L. C. and Hedenström, A. (2012). Vortex wake, downwash distribution, aerodynamic performance and wingbeat kinematics in slow-flying pied flycatchers. *J. R. Soc. Interface* **9**, 293–303.

Muijres, F. T., Elzinga, M. J., Melis, J. M. and Dickinson, M. H. (2014). Flies Evade Looming Targets by Executing Rapid Visually Directed Banked Turns. *Science* **344**, 172–177.

Muijres, F. T., Elzinga, M. J., Iwasaki, N. A. and Dickinson, M. H. (2015). Body saccades of *Drosophila* consist of stereotyped banked turns. *J. Exp. Biol.* **218**, 864–875.

Muijres, F. T., Iwasaki, N. N. A., Elzinga, M. J., Melis, J. M. and Dickinson, M. H. (2017). Flies compensate for unilateral wing damage through modular adjustments of wing and body kinematics. *Interface Focus* **7**, e0043411.

Murphy, M. E. and King, J. R. (1991). Protein intake and the dynamics of the postnuptial molt in White-crowned Sparrows, *Zonotrichia leucophrys gambelii*. *Can. J. Zool.* **69**, 2225–2229.

Murphy, M. E. and King, J. R. (1992). Energy and Nutrient Use during Moult by White-Crowned Sparrows Zonotrichia leucophrys gambelii. *Ornis Scand.* **23**, 304–313.

Nilsson, J.-A. and Svensson, E. (1996). The Cost of Reproduction: A New Link between Current Reproductive Effort and Future Reproductive Success. *Proc. Biol. Sci.* **263**, 711–714.

Norberg, U. M. (1975). Hovering flight in the pied flycatcher (*Ficedula hypoleuca*). *Swim. Fly. Nat.* **2**, 869–881.

Norberg, R. Å. (1994). Swallow tail streamer is a mechanical device for self-deflection of tail leading edge, enhancing aerodynamic efficiency and flight manoeuvrability. *Proc R Soc Lond B* **257**, 227–233.

Ouwehand, J., Ahola, M. P., Ausems, A. N. M. A., Bridge, E. S., Burgess, M., Hahn, S., Hewson, C. M., Klaassen, R. H. G., Laaksonen, T., Lampe, H. M., et al. (2016). Light-level geolocators reveal migratory connectivity in European populations of pied flycatchers *Ficedula hypoleuca*. *J. Avian Biol.* **47**, 69–83.

Pallas, P. S. (1764). Adumbratiunculae avium variarum praecedenti Elencho insertarum, sed quae in Systemate Naturae Illustl: Linnaei nondum extant.pp. 1–7.

Pap, P. L., Barta, Z., Tökölyi, J. and Vágási, I. C. (2007). Increase of feather quality during moult: A possible implication of feather deformities in the evolution of partial moult in the great tit Parus major. *J. Avian Biol.* **38**, 471–478.

R Core Team (2017). *R: A Language and Environment for Statistical Computing*. Vienna, Austria: R Foundation for Statistical Computing.

Swaddle, J. P. and Witter, M. S. (1997). The effects of molt on the flight performance, body mass, and behavior of European starlings (*Sturnus vulgaris*): An experimental approach. *Can. J. Zool. Rev. Can. Zool.* **75**, 1135–1146.

Swaddle, J. P., Witter, M. S., Cuthill, I. C., Budden, A. and McCowen, P. (1996). Plumage Condition Affects Flight Performance in Common Starlings: Implications for Developmental Homeostasis, Abrasion and Moult. *J. Avian Biol.* **27**, 103–111.

Swaddle, J. P., Williams, E. V. and Rayner, J. M. V (1999). The effect of simulated flight feather moult on escape take-off performance in starlings. *JAvian Biol* **30**, 351–358.

Thomas, A. L. R. (1993). On the aerodynamics of birds' tails. *Philos. Trans. Biol. Sci.* **340**, 361–380.

Thomas, A. L. R. (1996). The Flight of Birds that have Wings and a Tail: Variable Geometry Expands the Envelope of Flight Performance. *J. Theor. Biol.* **183**, 237–245.

Tobalske, B. W. and Dial, K. P. (1994). Neuromuscular Control and Kinematics of Intermitent Flight in Budgerigars (*Melopisttacus undulatus*). *J. Exp. Biol.* **187**, 1–18.

Tomotani, B. M., van der Jeugd, H., Gienapp, P., de la Hera, I., Pilzecker, J., Teichmann, C. and Visser, M. E. (2018a). Climate change leads to differential shifts in the timing of annual cycle stages in a migratory bird. *Glob. Change Biol.* **24**, 823–835.

Tomotani, B. M., Muijres, F. T., Koelman, J., Casagrande, S. and Visser, M. E. (2018b). Simulated moult reduces flight performance but overlap with breeding does not affect breeding success in a long-distance migrant. *Funct. Ecol.* **32**, 389–401.

Tucker, V. A. (1991). The effect of molting on the gliding performance of a Harris' Hawk (Parabuteo unicinctus). *The Auk* 108–113.

Usherwood, J. R. (2009). The aerodynamic forces and pressure distribution of a revolving pigeon wing. *Exp. Fluids* **46**, 991–1003.

Vágási, C. I., Pap, P. L., Vincze, O., Benkő, Z., Marton, A. and Barta, Z. (2012). Haste Makes Waste but Condition Matters: Molt Rate–Feather Quality Trade-Off in a Sedentary Songbird. *PLoS ONE* **7**, e40651.

Weber, T. P., Borgudd, J., Hedenström, A., Persson, K. and Sandberg, G. (2005). Resistance of flight feathers to mechanical fatigue covaries with moult strategy in two warbler species. *Biol. Lett.* **1**, 27–30.

Williams, E. V. and Swaddle, J. P. (2003). Moult, flight performance and wingbeat kinematics during take-off in European starlings *Sturnus vulgaris*. *J. Avian Biol.* **34**, 371–378.

Woltring and Huiskes (1990). Stereophotogrammetry. In *Biomechanics of Human Movement* (ed. Berme and Cappozzo).

Table 1: List of symbols and abbreviations.

Abbreviations		
P1-P8		first to eighth primary feathers
PC1-PC3		first to third principal components
T_{in}		inner wing triangle, spanned by shoulder, rump and P1 tip
T_{mid}		middle wing triangle, spanned by the shoulder, wrist and P1 tip
T_{out}		outer wing triangle, spanned by the wrist, wingtip and P4 tip
T_{gap}		molt gap wing triangle, spanned by the wrist, P1 tip and P4 tip
Symbols		
symbol	*unit*	*Description*
a	[m s^{-2}]	acceleration of the bird, as determined from the beak tip movement
b_{gap}	[m]	wing gap width, as defined by the distance between the P1 and P4 tip
b_{tail}	[m]	tail span, as defined by the distance between the tail tip markers
$C_{F\alpha}$	[-]	angle-of-attack-specific aerodynamic force coefficient of a bird wing
F	[-]	F-value for a linear mixed-effect model test
F	[N]	aerodynamic force vector
F	[N]	aerodynamic force scalar
F^{*}	[-]	weight-normalized aerodynamic force scalar
f	[s^{-1}]	wingbeat frequency
g	[-]	g-force, the non-dimensional unit of weight-normalized aerodynamic force
g	[m s^{-2}]	gravitational acceleration vector
g	[m s^{-2}]	gravitational acceleration scalar
m	[kg]	mass of the bird
n	[-]	sample size for a statistical test
p	[-]	p-value for a linear mixed-effect model test
S	[m^2]	Area
S_2	[m^4]	second-moment-of-area relative to the wing joint
t	[s]	time
U	[m s^{-1}]	velocity vector

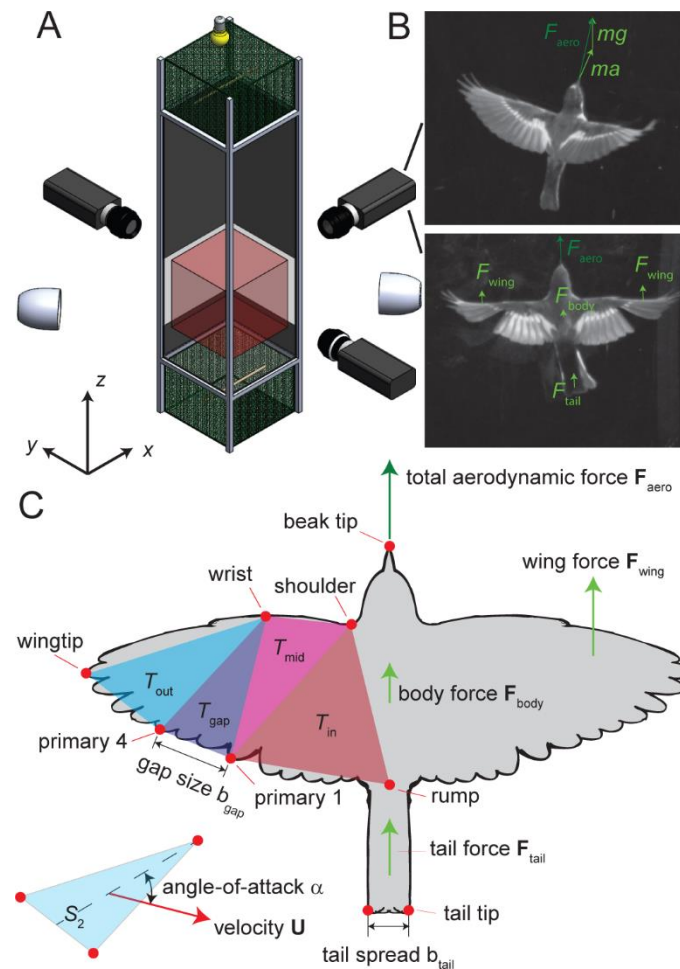| U	[m s^{-1}]	speed scalar
α	[°]	angle-of-attack
Δt	[s]	wingbeat-period
$\dot{\varphi}$	[rad s^{-1}]	angular wing stroke velocity
ρ	[kg m^{-3}]	air density
τ	[-]	wingbeat-period normalized time

Figures

Figure 1. Experimental setup, kinematics tracking parameters and modelled aerodynamic forces. (A) The experimental setup consists of a vertical flight tunnel, with release box and collection box in both ends, and a videography system consisting of three synchronized high-speed video cameras. (B) cropped videography images showing an upward flying *control* bird (top) and *molt* bird (bottom), including aerodynamic forces produced by each bird. (C) From the videography data, we tracked 14 natural markers on each bird: the tip of the beak, the rump, the left and right tail tip, and 6 markers on each wing. Based on these markers, we separated the wing into four triangles, for which we determined the second-moment-of-area, velocity and angle-of-attack throughout the flight trajectory. We estimated net total aerodynamic force ($\mathbf{F}_{aero}$) based on beak displacement, and modelled it as the sum of wing, body and tail forces ($\mathbf{F}_{wing}$, $\mathbf{F}_{body}$, $\mathbf{F}_{tail}$, respectively).
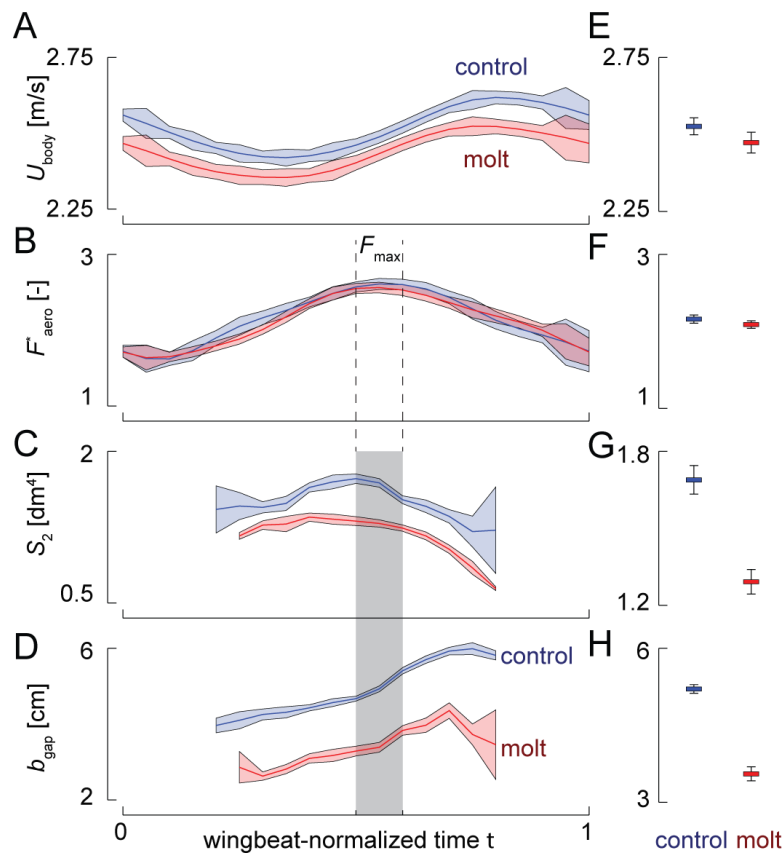
Figure 2. Flight performance and wing morphology metrics during the upward escape flight of pied flycatchers with and without wing molt gaps. (A-D) Temporal dynamics throughout the wingbeat of (A) flight speed, (B) weight-normalized aerodynamic force, (C) second-moment-of-area of the wings, and (D) molt gap size. Data for the *control* and *molt* group are shown in blue and red, respectively. For each group, the data is visualized as the temporal dynamics of mean and standard error, whereby the temporal resolution was similar to the video frame rate. Thus, for each wingbeat-normalized time bin the mean and standard error was calculated based on the data of that bin. (E-F) The mean and standard error of the wingbeat-average flight speed and normalized force production for the *control* and *molt* group, respectively. (G-H) The mean and standard error of second-moment-of-area and molt gap size within the wingbeat-normalized time-window $0.5<\tau<0.6$ (grey bar) where force production is maximal (B). Note that for the *control* birds, b_{gap} represents the wing width at location where the molt birds have a simulated molt gap. For flight speeds (A,E) and aerodynamic forces (B,F) the sample sizes are $n_{control}=73$ flights and $n_{molt}=73$ flights; for S_2 (C,G) and molt gap size (D,H) they are $n_{control}=66$ flights and $n_{molt}=65$ flights.
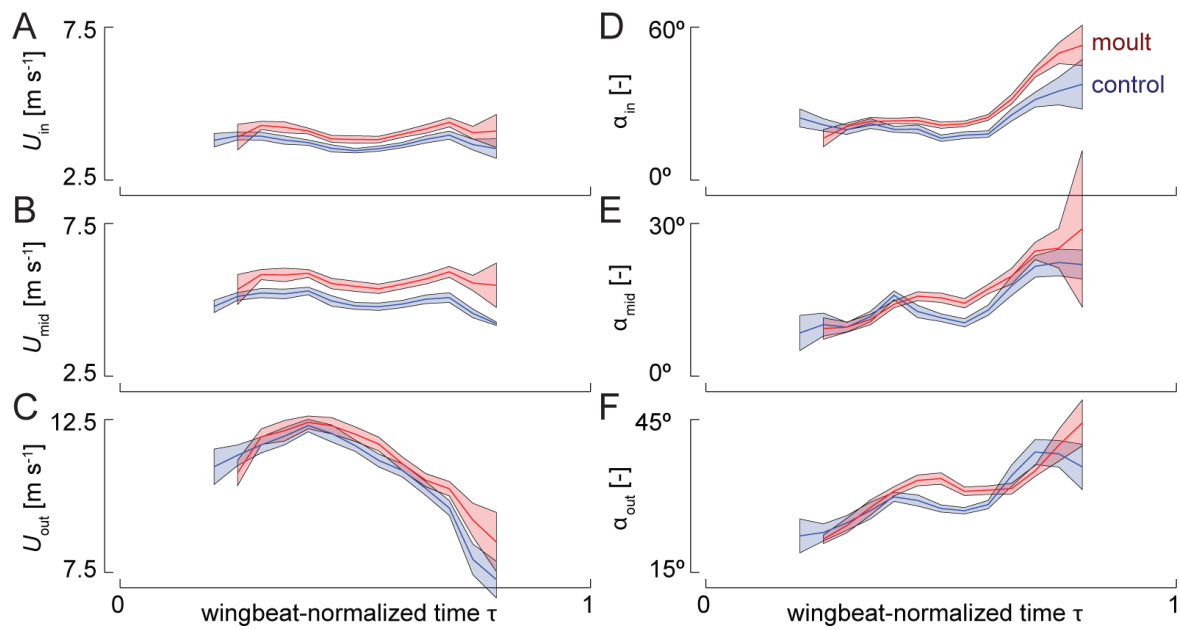
Figure 3. The speed and angle-of-attack of the different wing sections throughout the wingbeat of the upward escape flight of pied flycatchers with and without wing molt gaps. Data for the *control* group (*n*=66 flights) and *molt* group (*n*=65 flights) are shown in blue and red, respectively. For each group, data is shown as the average and standard error throughout wingbeat-normalized time, calculated as described for Fig. 2A-D. (A-C) temporal dynamics of the speed of the three wing sections: (A) inner wing, (B) mid wing, and (C) outer wing section, as defined in Fig. 1C. (D-F) Temporal dynamics of the angle-of-attack of the three wing sections: (A) inner wing, (B) mid wing, and (C) outer wing section, as defined in Fig. 1C.
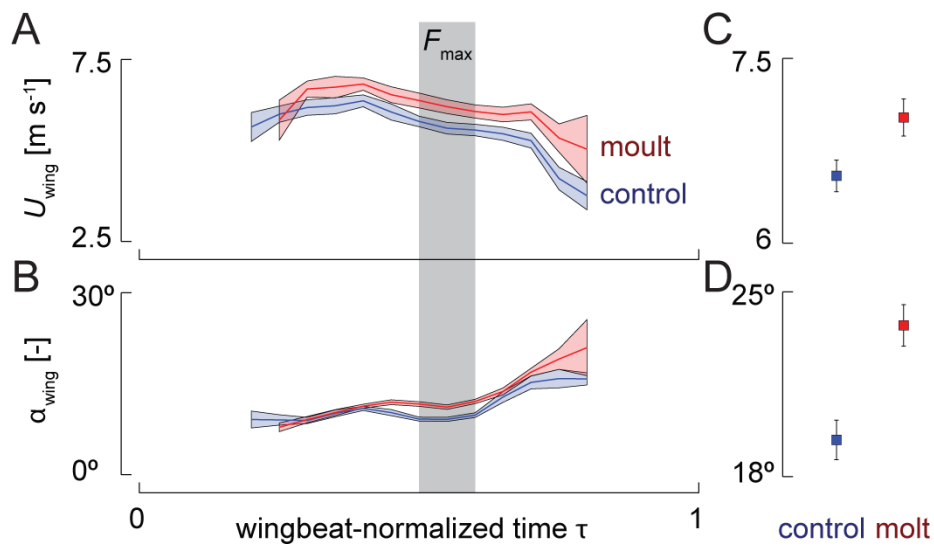
Figure 4. The mean speed and angle-of-attack of the wing during the upward escape flight of pied flycatchers with and without wing molt gaps. (A,B) the temporal dynamics of wing speed (A) and angle-of-attack (B) throughout the wingbeat. Data for the *control* and *molt* group are shown in blue and red, respectively. For each group, data is shown as the temporal distribution of means and standard errors throughout wingbeat-normalized time, at a temporal resolution similar to the video fame rate. (C,D) the mean and standard error of the mean wing speed (C) and angle-of-attack (D) within the wingbeat-normalized time-window $0.5 < \tau < 0.6$ (grey bar) where force production is maximal (Fig. 2B). All data was calculated as described in Fig. 2, and sample sizes were $n_{control}=66$ flights and $n_{molt}=65$ flights.
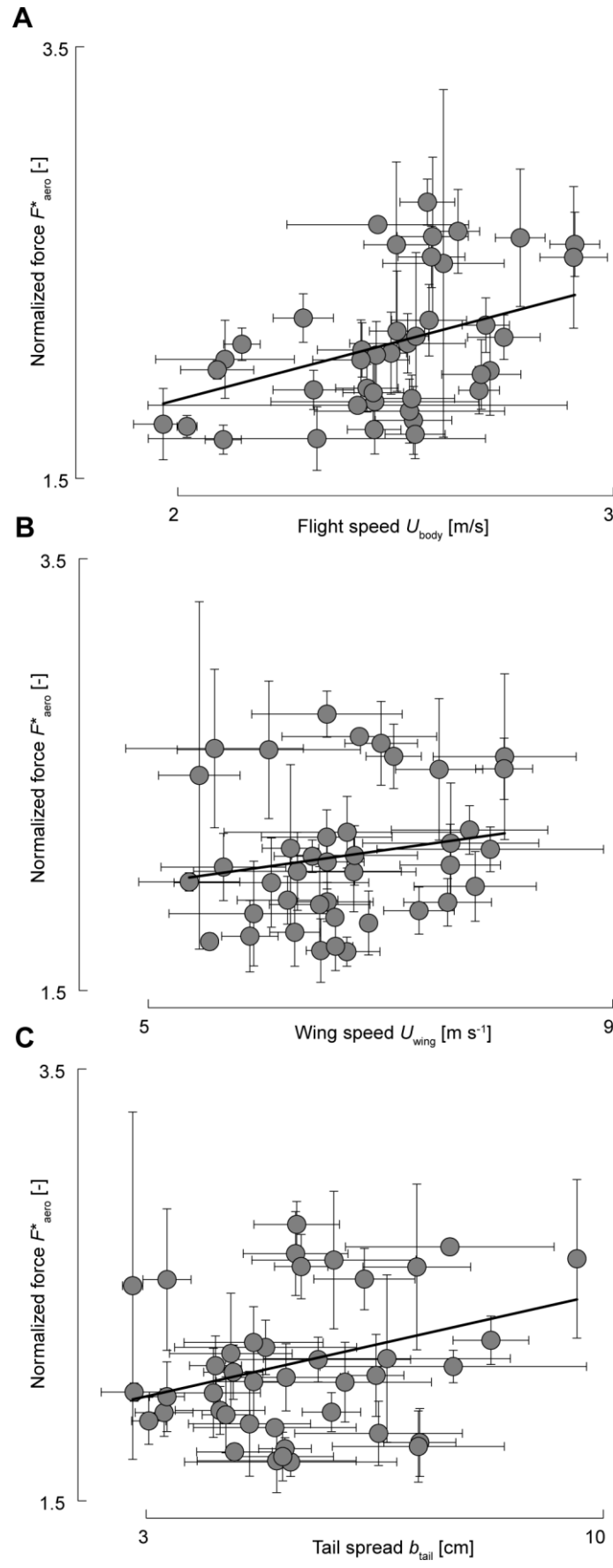
Figure 5. Relationship between weight-normalized aerodynamic force and flight speed, wing speed and tail spread throughout upward escape maneuvers of pied flycatchers. Normalized force is significantly correlated with wingbeat-average flight speed (A), mean wing speed (B) and tail spread (C) at maximum force production (within wingbeat-normalized time-window $0.5 < \tau < 0.6$). Each data point shows the mean and standard error for all wingbeats of an individual (see Database S1 for the number of wingbeats per individual). Black lines represent predictions of the linear mixed-effect models.
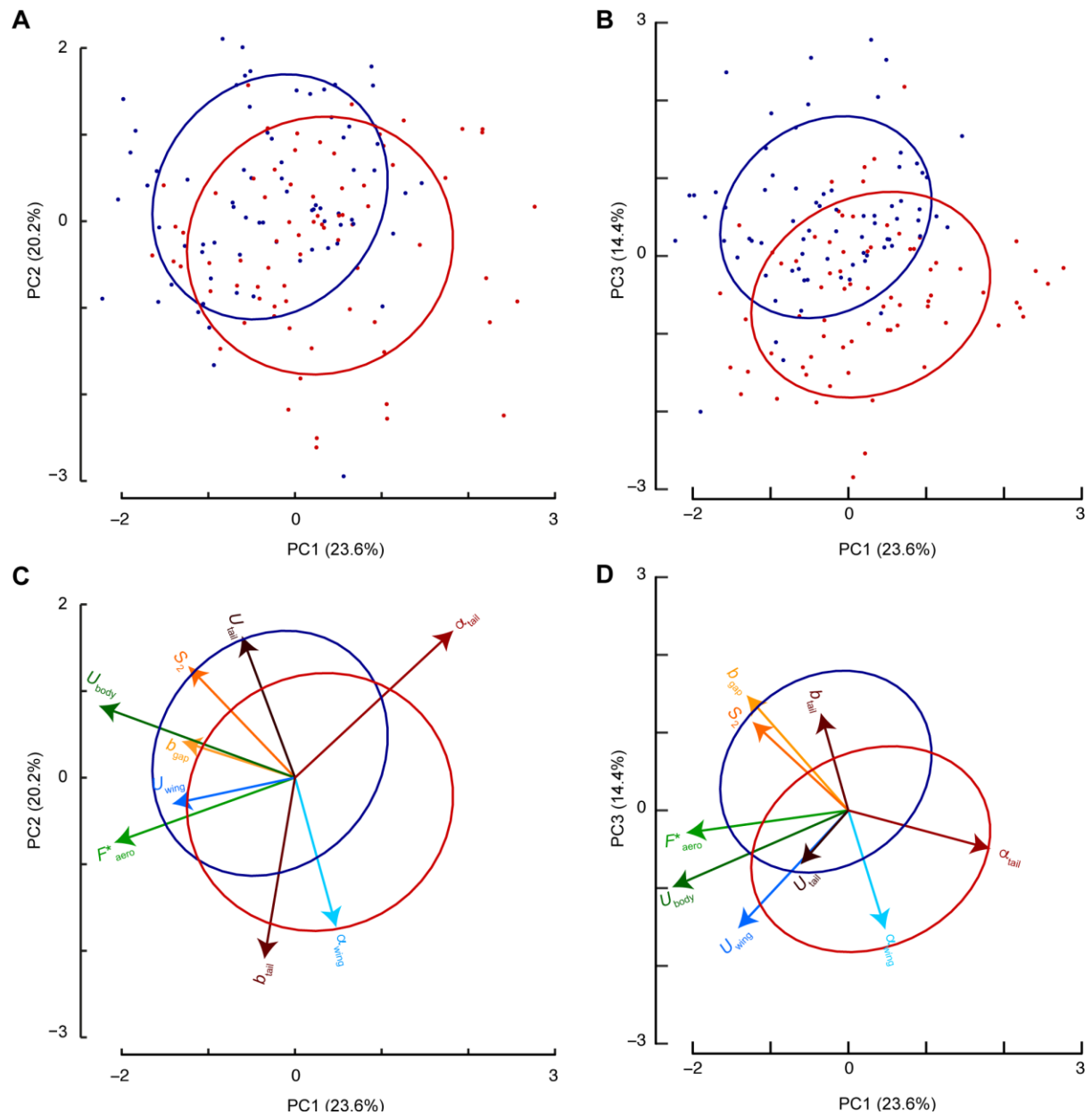
Figure 6. Principal component analysis results for the flight dynamics of upward escaping pied flycatchers with and without wing molt gaps. (A,B) The first, second and third principal component scores for all measured escape flights as depicted in the PC1-PC2 biplot (A) and PC1-PC3 biplot (B). Data of birds with and without a molt gap are in red and blue, respectively. (C,D) projection of the principal component vectors (loadings) of the tested parameters onto the PC1-PC2 biplot (C) and PC1-PC3 biplot (D). The tested parameters were weight-normalized aerodynamic force (light green), flight speed (dark green), the second-moment-of-area (dark orange), molt gap size (light orange), speed and angle-of-attack of the wing (dark and light blue, respectively), and speed, spread and angle-of-attack of the tail (dark, middle and light red, respectively). The blue and red circles represent normal data ellipses (68% probability) for the *control* and *molt* groups, respectively.
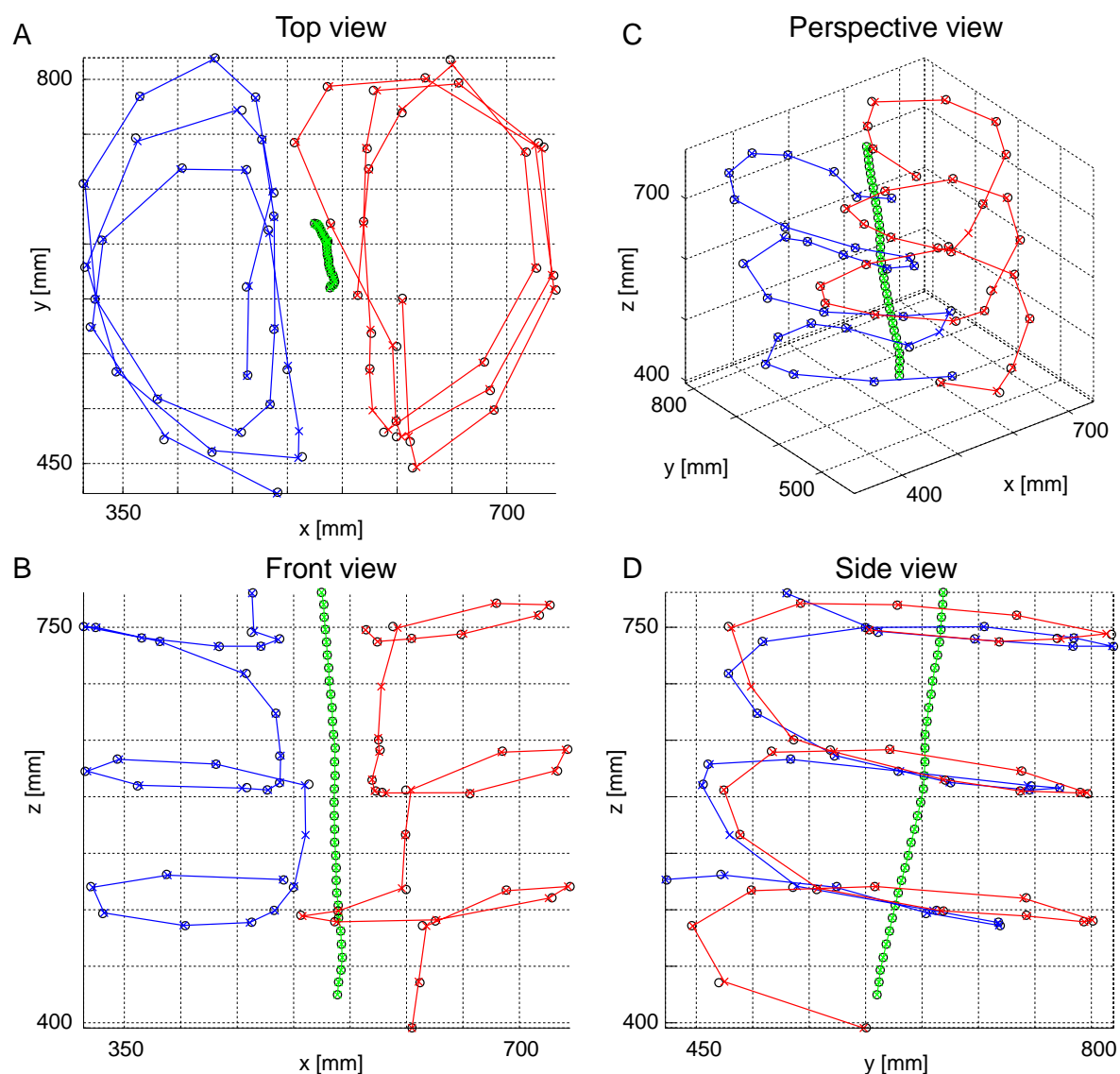
Figure S1: Beak and wingtip trajectories throughout the upward-directed escape maneuver of a pied flycatcher with simulated molt gaps. The trajectories are shown in the world reference from a top view (A), front view (B), perspective view (C) and side view (D). Beak movement is in green, left wingtip movement in blue and right wingtip movement in red. The crosses show the Kalman smoothed position at each video frame, whereas the corresponding back circles show the non-filtered position.

Table S1: Effects of treatments on several flight performance components. Statistics are given for the point of exclusion of each term from the model. Significant *p*-values are marked in bold, significance was assessed after a Holm-Bonferroni correction.

Gap width	Estimate	s.e.	ndf	ddf	*F*-test	*p*-value
Treatment			1.00	37.41	48.59	**<0.01**
Treatment (control)	5.24	0.17				
Treatment (molt)	3.55	0.18				
Normalized force	**Estimate**	**s.e.**	**ndf**	**ddf**	***F*-test**	***p*-value**
Treatment			1.00	37.89	0.69	0.41
Treatment (control)	2.16	0.07				
Treatment (molt)	2.08	0.07				
Second-moment-of-area	**Estimate**	**s.e.**	**ndf**	**ddf**	***F*-test**	***p*-value**
Treatment			1.00	35.72	20.61	**<0.01**
Treatment (control)	1.61	0.05				
Treatment (molt)	1.27	0.05				
Flight speed	**Estimate**	**s.e.**	**ndf**	**ddf**	***F*-test**	***p*-value**
Treatment			1.00	38.48	0.94	0.34
Treatment (control)	2.52	0.05				
Treatment (molt)	2.45	0.05				
Wing speed	**Estimate**	**s.e.**	**ndf**	**ddf**	***F*-test**	***p*-value**
Treatment			1.00	35.08	4.28	0.05
Treatment (control)	6.52	0.16				
Treatment (molt)	7.00	0.16				
Wing angle-of-attack	**Estimate**	**s.e.**	**ndf**	**ddf**	***F*-test**	***p*-value**
Treatment			1.00	33.20	15.78	**<0.01**
Treatment (control)	19.39	0.77				
Treatment (molt)	23.73	0.77				
Tail speed	**Estimate**	**s.e.**	**ndf**	**ddf**	***F*-test**	***p*-value**
Treatment			1.00	38.46	1.89	0.18
Treatment (control)	3.57	0.09				
Treatment (molt)	3.38	0.10				
Tail spread	**Estimate**	**s.e.**	**ndf**	**ddf**	***F*-test**	***p*-value**
Treatment				37.77	0.15	0.70
Treatment (control)	5.34	0.33				
Treatment (molt)	5.15	0.34				
Tail angle-of-attack	**Estimate**	**s.e.**	**ndf**	**ddf**	***F*-test**	***p*-value**
Treatment			1.00	38.47	0.47	0.50
Treatment (control)	30.79	2.90				
Treatment (molt)	33.69	3.05				

Table S2: Results of the multiple regression analysis testing the effect of various kinematic variables on the normalized force. Model selection was performed via backwards selection, dropping non-significant terms in each step. Statistics are given for the point of exclusion of each term from the model.

Normalized force	Estimate	s.e.	ndf	ddf	*F*-test	*p*-value
Second-moment-of-area	0.04	0.09	1.00	111.14	0.18	0.67
Flight speed	0.53	0.14	1.00	99.62	13.98	**<0.01**
Wing speed	0.08	0.03	1.00	126.86	6.12	**0.01**
Wing angle-of-attack	0.00	0.01	1.00	121.94	0.44	0.51
Tail speed	0.07	0.02	1.00	120.81	16.70	**<0.01**
Tail spread	0.07	0.02	1.00	90.59	0.69	0.41
Tail angle-of-attack	0.00	0.00	1.00	114.72	0.50	0.48

Table S3: Outcomes of the principal component analysis including loadings of morphology variable S_2, performance variable normalized force, and wing kinematics variables angles-of-attack and wing speed. We retained components that explained a variance larger than 1 (PC1 to 3).

	PC1	PC2	PC3	PC4	PC5	PC6	PC7	PC8	PC9
Standard deviation	1.42	1.32	1.11	0.99	0.87	0.82	0.74	0.62	0.50
Proportion of Variance	0.24	0.20	0.14	0.11	0.09	0.08	0.06	0.04	0.03
Cumulative Proportion	0.24	0.44	0.58	0.70	0.79	0.86	0.93	0.97	1.00
Variance explained	2.02	1.73	1.24	0.98	0.76	0.67	0.54	0.38	0.25
Gap width	-0.30	0.10	0.44	-0.11	0.04	-0.77	0.26	0.08	-0.14
Normalized Force	-0.48	-0.19	-0.08	-0.34	-0.15	0.36	0.67	-0.06	0.09
Second-moment-of-area	-0.28	0.32	0.34	0.14	-0.56	0.15	-0.26	-0.53	0.01
Flight speed	-0.52	0.21	-0.29	0.16	0.42	0.11	-0.16	-0.08	-0.59
Wing speed	-0.33	-0.08	-0.45	0.24	-0.54	-0.22	-0.17	0.50	0.10
Wing angle-of-attack	0.11	-0.43	-0.45	-0.19	-0.13	-0.39	-0.05	-0.61	-0.14
Tail speed	-0.14	0.41	-0.20	-0.72	0.12	-0.07	-0.35	0.04	0.34
Tail spread	-0.08	-0.52	0.37	-0.40	-0.14	0.17	-0.41	0.25	-0.39
Tail angle-of-attack	0.42	0.42	-0.15	-0.26	-0.38	0.03	0.26	0.14	-0.57

Table S4: Effects of treatment on the principal components 1 to 3. Statistics are given for the point of exclusion of each term from the model.

PC1	Estimate	s.e.	ndf	ddf	*F*-test	*p*-value
Treatment			1.00	38.45	6.88	**0.01**
Treatment (control)	-0.42	0.24				
Treatment (molt)	0.49	0.25				
PC2	**Estimate**	**s.e.**	**ndf**	**ddf**	***F*-test**	***p*-value**
Treatment			1.00	38.00	5.80	**0.02**
Treatment (control)	0.28	0.20				
Treatment (molt)	-0.43	0.21				
PC3	**Estimate**	**s.e.**	**ndf**	**ddf**	***F*-test**	***p*-value**
Treatment			1.00	37.83	26.32	**<0.01**
Treatment (control)	0.62	0.15				
Treatment (molt)	-0.50	0.16				

Movie 1: Three-camera stereoscopic video of a Pied Flycatcher from the *control* group performing an upward-directed escape flight maneuver. The video was recorded at 200 frames per second and replayed at 10 frames per second, and is thus slowed down 20 times.

Movie 2: Three-camera stereoscopic video of a Pied Flycatcher from the *molt* group performing an upward-directed escape flight maneuver. The video was recorded at 200 frames per second and replayed at 10 frames per second, and is thus slowed down 20 times.